Chemical Engineering Science 302 (2025) 120868

Contents lists available at ScienceDirect

Chemical Engineering Science

journal homepage: www.elsevier.com/locate/ces

3D printing of aligned silk fibroin microfibers covered with nitrogen-doped carbon dots for anti-counterfeiting

Anastasia Kryuchkova [1], Anna Ponomarets [1], Victoriia Suchilova, Egor Ryabchenko, Chantal Tracey, Pavel Krivoshapkin, Elena Krivoshapkina [*]

EnergyLab, ITMO University, 9 Lomonosova Street, Saint Petersburg 191002, Russian Federation

ARTICLE INFO

Keywords:
Silk
Fibroin
Alignment
3D printing
Optical properties
Microfibers
Anti-counterfeiting

ABSTRACT

Counterfeiting has serious economic and social consequences, prompting researchers worldwide to develop innovative and highly secure anti-counterfeiting methods, including the use of various polymer printing techniques and the integration of functional materials to create patterns with customized designs that are easy to detect and cannot be falsified. Composite inks made of silk fibroin microfibers and polyvinyl alcohol or polyethylene glycol were developed to produce patterns with the microstructures aligned in the direction of extrusion during the 3D printing process. Fibroin microfibers were obtained via high temperature treatment and used as a precursor for carbon dot synthesis. This approach allowed the microfiber structure to be maintained and be amenable to the synthesis of carbon dots doped with N-heteroatom on its surface, resulting in a material that fluoresces bright blue when irradiated at 365 nm but remains invisible in normal lighting conditions.

1. Introduction

The counterfeiting of pharmaceutical and food products is particularly concerning because the lack of proper controls in supply chains can jeopardise public health and safety when such goods bypass quality checks and certifications (Yoon et al., 2013). As such, one of the main goals of contemporary anti-counterfeiting is the development of systems with advanced features that can generate security codes and/or markers that are impossible to replicate. Of the many methods developed so far, the use of advanced luminescent materials in security 3D printing shows significant potential. While luminescent tags and labels have are common anti-counterfeiting measures, they can be copied due to their predictable encoding methods. Recent studies suggest that 3D-printed structures with unique shapes could address this problem.

3D-printed structures are highly suited to the high-speed manufacturing of high-end security markers because they are easily scalable; readily produced under industrial conditions; and can be applied on surfaces of various shapes, sizes, and geometries at relatively low temperatures and non-specific settings (Muthamma et al., 2021). Since its inception, three-dimensional printing technology has evolved from the layer-by-layer creation of physical structures based on computer-aided design drawings (Tofail et al., 2018). Today, the complexity of tasks and structures undertaken by 3D printing has undergone significant technological advancements, which now allows for the creation of advanced materials and devices such as sensors (Jarošová et al., 2019), self-powered systems (Lin et al., 2019), remote communication sensors (Krykpayev et al., 2017), and enables applications in the Internet of Things (Yin et al., 2016).

The use of inkjet and 3D inkjet printing in biotechnology (Hussin et al., 2021), biosensing (Li et al., 2015), and diagnostics (Rosati et al., 2022) has seen significant progress over the last decade – especially in terms of the development of customised inks from a broad selection of materials. Unfortunately, the majority of these inks quickly lose their functional properties during degradation, and tend to be toxic (Guo and Ma, 2014; Seal et al., 2001). Furthermore, problems associated with ink stability, the mechanical and storage stability of printed patterns at room temperature, and the implementation of functional properties remain unresolved (Qiu et al., 2022). The latter is often attributed to the non-uniform distribution of functional materials throughout the ink, which results in the deterioration of rheological characteristics (West and Hubbell, 1999).

Studies have shown that stimuli-responsive luminescent tags have the ability to show encrypted messages under certain lighting and are flexible and easy to integrate in packaging or products, making them

* Corresponding author.
E-mail address: kef@scamt-itmo.ru (E. Krivoshapkina).
[1] These authors contributed equally.

https://doi.org/10.1016/j.ces.2024.120868
Received 1 July 2024; Received in revised form 22 September 2024; Accepted 22 October 2024
Available online 28 October 2024

highly suited for security and authentication purposes (Gao et al., 2019). Such tags can be obtained using luminescent nanoparticles such as semiconductor nanocrystals (Han et al., 2017; Sun et al., 2012), inorganic perovskite nanocrystals (Kalytchuk et al., 2018), rare-earth-doped nanostructures (Gupta et al., 2010), polymer nanoparticles (Chang et al., 2014; Peng et al., 2016), hybrid materials (Kaczmarek et al., 2017; Ma et al., 2018), and carbon dots (Jiang et al., 2017, 2016; Song et al., 2016). These optically active, functional nanoparticles can be easily incorporated into suitable polymer matrices to create viable inks whose optical, mechanical, and rheological properties can be controlled, enabling the creation of luminescent security tags for product authentication (Blanco, 2020; Sai Saran et al., 2022).

Carbon dots (CDs) are considered highly promising luminescent nanomaterials for anti-counterfeiting applications due to their strong fluorescence (PL) and non-toxic nature (Hola et al., 2014; Zhang and Yu, 2016). CDs have garnered substantial interest across various industries due to their appealing functional characteristics, including strong luminescence, high photo- and chemical stability, and low toxicity. They have found application across a wide range of technologies, including light-emitting devices (Zhang et al., 2013), water splitting (Fernando et al., 2015), catalysis (Du and Guo, 2016), and various biomedical applications like cellular optical imaging, biosensing, photothermal therapy, and drug delivery (Luo et al., 2013; Peng et al., 2017). Recent studies have also demonstrated the potential of invisible CD luminescent tags for anti-counterfeiting purposes (Jiang et al., 2016; Qu et al., 2012; Song et al., 2016). A clear advantage exists for the use of CDs as the way to control the optical properties of printed patterns by using environmentally friendly nanoparticles sourced from natural materials that are safe and efficient and can be effectively utilised in the pharmaceutical and/or food industries (Jiang et al., 2015; Li et al., 2010; Muthamma et al., 2021; Tomal et al., 2021; Wang et al., 2017).

In this work, we developed a simple and green approach to creating anti-counterfeiting labels by combining 3D printing technology and creating optically active *Bombyx mori* (*B. mori*) silk fibroin microfibers (FMF) coated with CDs. To effectively create optically active tags for anti-counterfeit purposes, CD serves as the primary optically active agent, while silk fibers provide a carbon source and substrate. *B. mori* are a type of *Lepidoptera* insect (Singh and Jayasomu, 2002), and its silk, a natural macromolecular protein, has a broad range of applications (Tracey et al., 2023; Yao et al., 2022). Due to its biocompatibility, biodegradability, and excellent mechanical properties as well as the ability to process it into multiscale dimensions, silk fibroin (SF) is widely used in traditional textiles; advanced sectors like optics, electronics, biomedicine; and environmental engineering (Molinnus et al., 2021; Tao et al., 2012; Wang et al., 2023). In addition to acting as a substrate, silk also served as the carbon source for CDs because, in addition to being simple, quick, eco-friendly, and cost-effective, the technical processes required for the alteration are also preserve the original characteristics of the silk (Zhang et al., 2015). It is hypothesised that functional composite materials suitable for aligned 3D printing can be created using silk microfibres, which will be oriented in the direction of extrusion. Ensuring that the microfibers are oriented in the direction specified by the user is crucial for producing polymer-matrix composites with customised attributes. We used a unique approach that allows us to use the functional groups on the silk surface as nucleation points for CDs, which leads to their strong crosslinking to the silk surface and prevents their leaching, minimising their chances of contaminating the protected product. Using such an approach, we developed a custom fluorescent FMF-based ink. Using extrusion-based 3D printing enabled FMF alignment, which allowed the creation of encrypted, stimuli-responsive luminescent tags. The chosen polymer materials for extrusion-based printing were selected based on their low polydispersity, ensuring the preservation of CD optical properties, as well as their favorable printability and film-forming abilities.

The CD/FMF ink fluoresces vivid blue upon irradiation with ultraviolet (UV) light with an excitation wavelength of 365 nm UV light but is invisible in daylight. Not only do their notable characteristics, such as intense and stable fluorescence, minimal toxicity, and affordability, make them a promising option for fluorescent ink in anti-counterfeiting, but this innovative technique allows for the creation of intricate and personalized structures based on a pattern of aligned FMF, enabling the production of a wide range of unique designs.

2. Experimental methods

2.1. Materials

Polyvinyl alcohol (PVA, 95.0 %) and glycerol ($C_3H_8O_3$, 99.5 %) were obtained from LenReaktiv (Russia). Polyethylene glycol 4000 (PEG-4000) and sodium carbonate (Na_2CO_3, 99.0 %) were purchased from Sigma-Aldrich. Urea ($CO(NH_2)_2$, $\geq$99.8 %) and hydrochloric acid (HCl, 36 %) were acquired from NevaReaktiv (Russia). Isopropyl alcohol (IPA, 99.8 %) was purchased from Ecos-1. All chemicals from commercial sources were used without further purification. Milli-Q deionized (DI) water (15 MΩ·cm resistivity) was used in all experiments unless otherwise stated. The IMTHAILAND Company supplied *B. mori* cocoons, which consist of completely natural silkworm silk.

2.2. Purification of B. mori silk cocoons

B. mori cocoons were cut into small pieces (1 – 5 cm) before being degummed by boiling them in 0.02 M Na_2CO_3 solution (1 % w/v) at 90 °C under continuous stirring for 90 min, and then washed with deionized water (Roblin et al., 2023). Following that, the degummed silk pieces were introduced to a 1 M HCl solution (5 % w/v) at 40 °C and sonicated for 4 h before being dried at 60 °C for 12 h (Kiseleva et al., 2021).

2.3. Preparation of FMF covered with N-doped CD

The synthesis technique described by Tian et al. (Tian et al., 2017) was modified to produce *B. mori* FMFs covered with CDs. This method allows to synthesize N-doped CD in-situ during the formation of the FMF. Fig. 1 illustrates the synthetic procedure. Briefly, silk (0.5 g), urea (2 g), and water (10 mL) were made to react at 160 °C for 4 h under hydrothermal conditions in a 20 mL Teflon-lined stainless-steel autoclave and then allowed to cool room temperature. The precipitate was collected, dispersed in IPA, and centrifuged (8000 rpm, 10 min) four times to remove residual solvents and small organic molecules.

2.4. Preparation of FMF-based composite inks for 3D printing

Two types of inks were developed for the creation of suitable anti-counterfeiting tags. An aqueous suspension of FMF was used. The concentration of FMF was determined using a Goryaev camera and amounted to 367 200 microfibers in 1 μL of water (*i.e.*, 40 wt%). The first ink was made by dissolving PVA in deionized water at 80 °C under constant stirring to obtain an 8 wt% solution that was then mixed with the aqueous FMF suspension to obtain 1 wt% FMF-PVA. For the second ink, PEG-4000 was melted at 45 °C under stirring and mixed with 4 mL of the aqueous FMF suspension to obtain 10 wt% FMF-PEG. Both inks were stored in a dark place at room temperature until further use.

2.5. Anti-counterfeiting tag fabrication

Anti-counterfeit tags were fabricated using two extrusion approaches: extrusion-based 3D printing and using a syringe. In the first approach, a Cellink BIO X printer (CELLINK AB, Sweden) was used to extrude the FMF-PEG ink with the assistance of the open-source software Tinkercad. Briefly, 1.5 mL of FMF-PEG was put in a Nordson syringe and attached to the Cellink BIO X printer via the pneumatic syringe holder. A glass slide (Hermeon, Film Dressings, 76 × 26 × 1 mm) was placed into

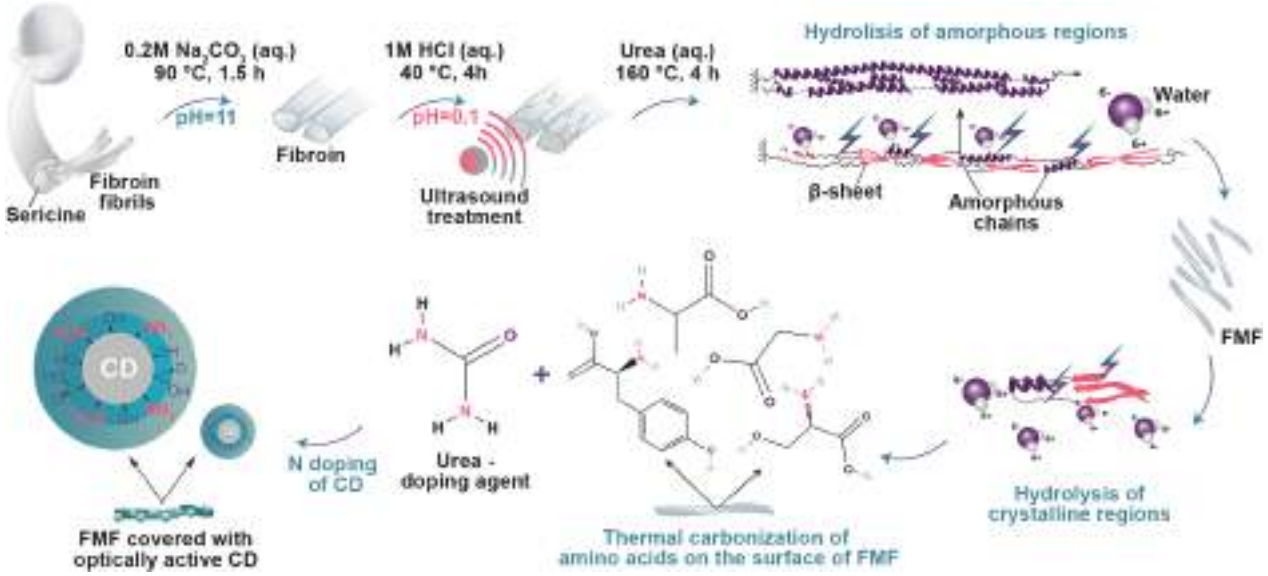

Fig. 1. Complex approach to the mechanism of optically active FMF formation.

the bioprinter plate holder. The ink was extruded onto the glass slide at a speed of 10 mm/s and pressure of 48 kPa using 250 μm syringe tips. To ensure appropriate printing conditions, the printhead was heated to 50 °C, as well as the printing temperature was cooled down to 16 °C. In the second approach, a BD Micro Fine Plus syringe with a 30G needle (external diameter of 0.30 mm) was to extrude the FMF-PVA ink. FMF-PVA was slowly and carefully extruded out of the syringe by hand to completely coat the solidified FMF-PEG structure on the glass slide to make it invisible under natural light.

2.6. Characterisation

The morphologies of both native SF and FMF were studied using scanning electron microscopy (SEM). SEM micrographs of the samples were obtained using a Vega Tescan 3 (SBH, Czech Republic) at an operating voltage of 2 kV with the samples fixed on carbon tape. Composition analyses were conducted using energy-dispersive X-ray (EDX) spectroscopy equipped with an X-ACT EDX detector from Oxford Instruments, Inc. Examination of the structure of the printed FMF objects was conducted using a Levenhuk DTX RC2 Digital Microscope (Levenhuk, Russian Federation). The size distribution of 400 FMF was analyzed using 10 SEM images and ImageJ image analysis software.

Fourier transform infrared (FTIR) spectroscopy was used to investigate the secondary structure of silk. FTIR spectra were acquired using a Thermo Scientific Nicolet iS5 FTIR spectrometer in the absorbance mode over a range of 4000–500 cm^{-1}. Dry samples were mixed with crystalline KBr (1 mg of the sample:199 mg of KBr) and then pressed into pellets. The data were collected with a resolution of 0.5 cm^{-1} using 20 scans and achieving a signal-to-noise ratio of 40 000:1. Manufacturer-provided Omnic 9 software was utilized to process the data, with background collection occurring prior to the accumulation of FTIR spectra from the samples.

The secondary structure of proteins was determined by amide I peak deconvolution using the method described by Madurga et al. (Madurga et al., 2017). The amide I and II peaks were fitted using Gaussian functions, with initial conditions determined based on the second derivative of the experimental spectrum. The minima of the second derivative were used to determine the number and positions of the Gaussian functions for fitting. The initial full width at half maximum was set and fixed at 8 cm^{-1}, and peak positions were fixed for all Gaussians used in the fitting. The fitting was completed after a linear baseline was applied. The fitting was consistently done using Omnic 9 software in all instances. The areas of the Gaussians were then used to estimate the content of different secondary structures based on the band assignments provided in Table 1.

Fluorescent microscopy images showing the PL of microfibers in contrast to native SF were obtained on an inverted Leica DMi8 microscope using a × 10 objective in DAPI, Rhodamine, and FTIC filters. The PL excitation and emission spectra of FMF were obtained using a Tecan Spark multimode microplate reader from Tecan Group Ltd. based in Switzerland.

The rheological behaviours of the FMF-PVA and FMF-PEG inks were analyzed by measuring the shear viscosity at different shear rates using a rheometer (AR-2000, TA Instruments, New Castle, DE, USA) equipped with a 40 mm/2° tapered plate at 20 °C and 40 °C, respectively. The temperatures were chosen based on the most clearly observed graph structures.

To determine the Young's modulus of FMF-PEG and FMF-PVA, strain sweep and frequency sweep experiments were conducted. In the strain sweep experiments, frequency was held constant at 1 Hz while strain varied from 15 % to 50 %. Conversely, frequency sweep experiments were performed at a constant strain of 1 % while frequency varied from 1 Hz to 100 Hz. The obtained elastic and viscous moduli (G' and G″, respectively) were then used to calculate the shear modulus.

The shear modulus of both inks was calculated as $G = \sqrt{G'^2 + G''^2}$.

Table 1
Vibrational band assignment in the amide I and II regions.

Wavenumber (cm^{-1})	Assignment	References
1475, 1490	CH_2, CH_3 bending in alanine	(Koperska et al., 2014)
1501	amide II, β-sheets	(Geminiani et al., 2023)
1539	amide II, α-helix/ random coil	(Geminiani et al., 2023)
1610–1620	Aggregated β-strand/ intermolecular β-sheet	(Jung, 2000), (Jackson and Mantsch, 1995), (Tretinnikov and Tamada, 2001), (Taddei and Monti, 2005)
1638–1655	random coil	(Teramoto and Miyazawa, 2005), (Tretinnikov and Tamada, 2001)
1663–1694	β-turn	(Mouro et al., 1997), (Tretinnikov and Tamada, 2001), (Taddei and Monti, 2005), (Dong et al., 1990), (Wilson et al., 2000)
1728	ν(C = O) amide I bond, β-sheets	(Geminiani et al., 2023)

Youngs modulus was determined as

$$E = 2G(1+\nu)$$

Were Poisson ration (ν), was approximated to 0.5.

3. Results and discussion

3.1. Formation of FMFs covered with N-doped CDs

In this paper, optically active FMFs capable of alignment during 3D printing were obtained via hydrothermal synthesis. First, the fibers were treated with a solution of Na_2CO_3 at about 90 °C for 90 min, which is the typical alkali degumming process (Horan et al., 2005; Kim et al., 2005; Li et al., 2003). Silk fibers consist of two proteins arranged in a core–-shell structure, with internal fibroin fibers being held together by an outer layer of sericin (Koh et al., 2015; Qi et al., 2017). Fibroin provides structural support and unique mechanical properties to silk while sericin acts as a binding agent during cocoon formation (Vepari and Kaplan, 2007). Depending on the type of silk, sericin can make up 25–30 % of the cocoon weight, with fibroin accounting for the remainder (Seo et al., 2023). The separation of these proteins through degumming, where sericin is dissolved in a chemical bath leaving fibroin almost intact, influences mechanical properties and standardizes material quality (Johansson et al., 1985; Kasoju and Bora, 2012). Degumming, which depends on Na_2CO_3 concentration and processing conditions (Dou and Zuo, 2015), removes sericin by dispersing, solubilizing, and hydrolysing sericin polypeptides (Sahoo et al., 2010). It should be noted that degumming can also be performed using acids. The effectiveness of removing sericin through the use of acids and alkalis can be attributed to the fact that sericin is an amphoteric protein with an isoelectric point between 3.9 and 4.3 (Ma et al., 2022; Zhou et al., 2014). As a result, the solubility of sericin is greatly influenced by the pH of the solution. The degumming process is accelerated in both highly alkaline and extremely acidic solutions. Sericin, being amphoteric, can form ionizable salts with acids and alkalis, leading to increased solubility (Haggag et al., 2007). Studies have shown that degumming has negligible impact on fibroin structure (Lucas et al., 1958; Pérez-Rigueiro et al., 2002). After degumming, haphazardly arranged individual fibroin fibrils became prominently visible. Additionally, internal voids and cracks formed in the cross-section of the fibers (**Figure S1**), which made silk fibroin (SF) more brittle. As long as there is a sericin layer protecting the inner protein chain, SF will remain structurally sound; however, once the alkaline solution comes in contact with fibroin, the integrity of the SF structure can be affected (Bucciarelli et al., 2021). It should be noted that the SF structure can begin to degrade before sericin is completely removed.

The next step in the preparation of SF was a 4 h ultrasound treatment in 1 M HCl solution to prepare SF for high-temperature processing by additional hydrolysis and removal of sericin residues that were not removed during alkaline degumming. Sonication, which can trigger various chemical and physical transformations in polymers (Wang et al., 2015), generated a highly intense physical setting and prepared SF for the production of microfibers (Zhu et al., 2022). This intense physical environment can later enable modifications to the secondary structure of SF under elevated temperatures during hydrothermal treatment.

Following four hours of continuous hydrothermal treatment, SF underwent a complete transformation into almost uniform FMF. This suggests that hydrolysis under critical high temperature conditions plays a crucial role in the degradation of fibroin fibers into FMF, particularly during hydrothermal treatment at 160 °C. Such reaction conditions were essential for keeping FMF integrity during subsequent synthesis of CD directly on their surface, preventing complete FMF decomposition. It is possible to suggest that there is a step-by-step degradation of SF areas that are more susceptible to hydrolysis, like the non-crystalline sections (Mandal et al., 2012). SF primarily consists of the amino acids glycine (Gly), alanine (Ala), serine (Ser), and tyrosine (Tyr), which make up about 90 % of the structure and are arranged in repetitive sequences with weak chemical bonds (Chen et al., 2012; Guo et al., 2018). During the initial stage of hydrolysis, the sericin remaining after degumming dissolves due to its strong solvation by water (Li et al., 2013; Wang et al., 2021; Zhang et al., 2014) while hydroxyl ions break the network of hydrogen bonds of amorphous random regions, resulting in the formation of FMF (Jia et al., 2021). Over time, the structures dominated by amorphous and crystal forms gradually begin to hydrolyse into small amino acids due to the strong solvation effect and high reactivity of water molecules towards weak chemical bonds (*e.g.*, ester or amido bonds) under subcritical conditions (Quitain et al., 2006). Since the number of available reaction sites of such amino acids as Gly, Ala, Ser, and Tyr on the FMF surface increases, these amino acids serve as *in situ* molecular precursors for carbon nanomaterials, acting as both a carbon source and a support material (Titirici and Antonietti, 2010). These surface SF moieties reacted with urea, which acted as a N source for CD heteroatom doping (Chekini et al., 2020; Maltseva et al., 2022). Urea and fibroin amino acids form a nanoplate structure through intermolecular H-bonding that then undergoes dehydration to create nitrogen-rich CDs with carboxyl, hydroxyl, and amide groups on the surface under hydrothermal conditions (Tian et al., 2017). While urea served as a doping agent, any additional impact on the extent of dehydration and carbonization between fibroin and urea depends on the solvent. The degrees of dehydration and carbonization increase gradually in water, leading to an increase in sp^2-domains and a violet–blue shift in CD absorption and emission bands (Yan et al., 2020). As intermolecular dehydration and hydrothermal carbonization progress on the FMF surface, uniform CDs are eventually formed, covering the surface of the resulting silk fibroin microrods. **Figure S2** shows SEM images of silk fibroin after the same synthesis without urea.

3.2. Characterization of native SF and FMF

SEM was used to observe the morphologies of SF and FMF and to measure their apparent sizes. The results displayed in Fig. 2**A** indicate that the shape of SF is relatively uniform, but not completely circular. Additionally, the image shows that SF coils in a helix around its axis. The diameter of the silk threads produced by silkworms ranges from 10 to slightly less than 20 μm, as observed through SEM imaging (Fig. 2**A**), and is not visibly altered by the solvent treatment used in the degumming process. SEM images of FMF in Fig. 2**B** show that the silk retain their microfibrous structures, unlike conventional silk solutions, which consist of particles of varying sizes. When compared to native SF, FMF had the same diameter (10 – 20 μm) but was notably shorter in length, ranging from 20 to 110 μm. Fig. 2**C** shows that FMFs have a wide size distribution with a peak at 64 μm.

EDX analysis was used to study the chemical compositions of SF (**Fig. S3A,B**) and FMF (Fig. S3**C,D**) and to verify the existence of N-doped CDs on the FMF surface. While both EDX mapping images confirm the presence of nitrogen, the levels were found to be greater in FMF compared to SF. This higher nitrogen content may be attributed to the effective formation of N-doped CDs on the FMF surface. It indicates that CD containing N-heteroatoms can be produced on FMF surfaces without complete destruction of SF from carbon in protein residues and nitrogen in urea.

FTIR was used to compare the molecular structures of native SF and FMF. Both the spectra of SF (**Fig. S4A**) and FMF (**Fig. S4B**) showed numerous peaks related to protein content, including amide I, II, and III bands at 1620, 1510, and 1226 cm^{-1} for SF and 1626, 1521 and 1229 cm^{-1} for FMF. Amide I is the most intense peak in the FMF FTIR spectrum and corresponds to the stretching vibration of the C = O bond in the peptide backbone (Taddei et al., 2016; Teramoto and Miyazawa, 2005; Van De Weert et al., 2001). The amide II band for FMF is noticeably smaller than that of native SF, which may be attributed to a combination of fewer bending vibrations of the N-H bond and the stretching vibration of the C-N bond in the peptide backbone

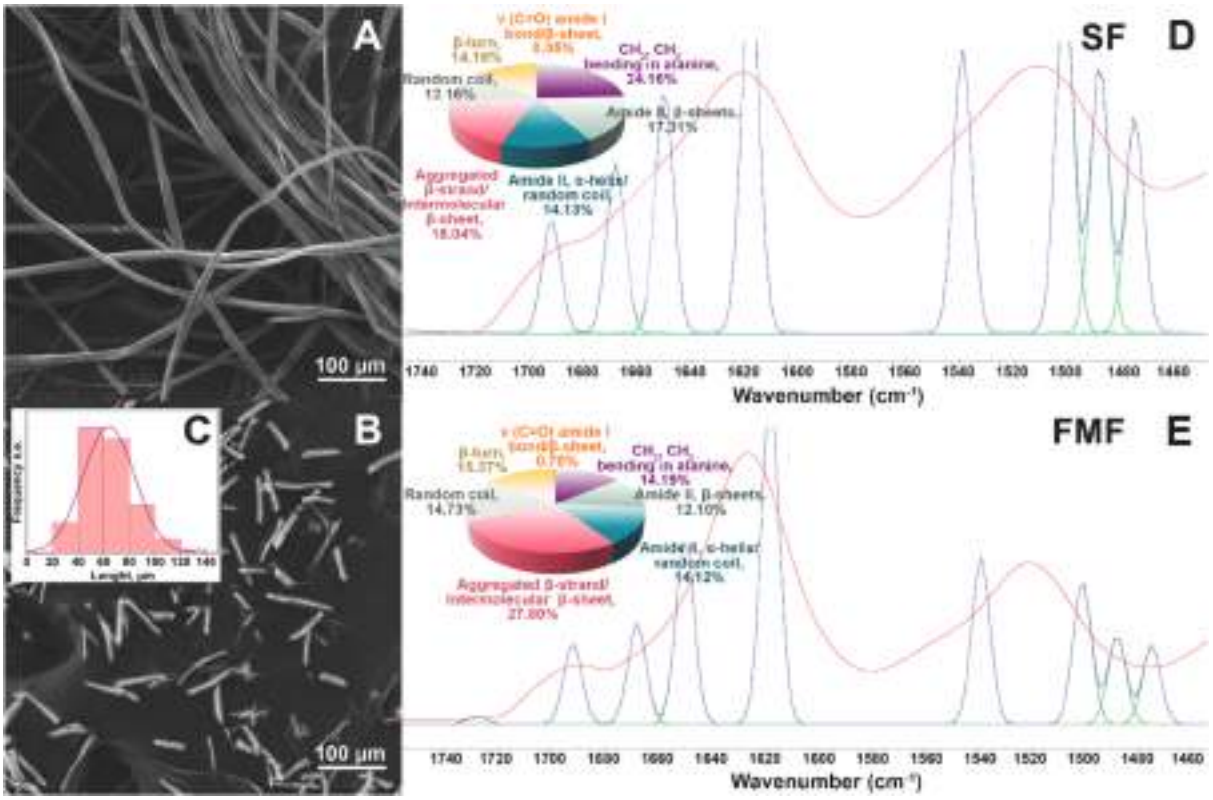

Fig. 2. SEM images of (A) SF and (B) FMF. (C) Size distribution of FMF. FTIR deconvoluted amide I and II bands and percentage of structures in (D) SF and (E) FMF.

(Kryuchkova et al., 2023). The FMF spectrum was characterized by the strong O-H stretching (3000–3600 cm^{-1}) band of water (Laity et al., 2015), which was the predominant component when compared with the SF band at 3130 – 3350 cm^{-1}. The peaks at around 1062 and 1401 cm^{-1} in the SF spectrum and 1042 and 1444 cm^{-1} in the FMF spectrum can be attributed to the C-O stretching and C-O-H bending vibrations of serine (Barth, 2000; Teramoto and Miyazawa, 2005), which accounts for approximately 12 % of the amino acids in *B. mori* fibroin (Gamo et al., 1977; Lucas et al., 1960). The minor peak at 3064 cm^{-1} in the SF spectrum could be linked to the aromatic C-H stretching band of tyrosine (Kumar et al., 2011), which makes up about 5 % of the amino acids in *B. mori* silk proteins (Gamo et al., 1977). This peak was not present in FMF. These differences suggest a higher proportion of tyrosine in SF compared to FMF, which agreed qualitatively with our suggestions of the FMF formation process in which a significant part of tyrosine is hydrolysed.

Deconvolution of the FTIR spectra (Fig. 2**D,E**) shows a diverse set of secondary structures in SF and FMF. β-sheets of amide I and II are predominant (~35-40 %), followed by random coils, α-helices, and β-turns. Also, peak fitting for both SF and FMF shows the content of CH_2, CH_3 bending in alanine, which is 24.16 % for SF and 14.19 % for FMF. Basically, the main difference in the content of secondary structures in SF and FMF is the different ratios of amorphous to crystalline phase between amides I and II, despite the fact that the total β-sheets ratio is approximately the same for both samples. as illustrated by the diagrams in Fig. 2**D,E**.

FMF PL was investigated using a Leica optical microscope with PL filters and the images are shown in Fig. 3**A-F, H-J**. The results showed that the fibroin microstructures exhibited bright PL in Rhodamine, FITC, and DAPI filters (Fig. 3**E-F**), while native SF does not fluoresce (Fig. 3**B-C**). In order to reveal the nature of PL and to make sure that the PL signal does not come from fibroin proteins but from CDs, we repeated the synthesis excluding urea as a doping agent. Fig. 3**H-J** shows FMF formed at the carbonisation stage. The resulting FMF exhibit identical morphology to FMF covered with N-doped CDs, but do not show any PL.

As such, it was concluded that the PL of FMF is associated with the formation of CDs on the FMF surface and is associated with electronic transitions of conjugated π domains in the sp^2 hybridized core and surface defects, such as imperfect sp^2 hybridized domains, sp^3 hybridized carbon atoms, and surface functional groups, of fibroin. To explore the optical properties of FMF in more detail, the photoluminescence (PL) spectra were recorded. The results in Fig. 3**G** indicate that when excited with a wavelength of 334 nm, the sample exhibits its highest PL emission intensity at 413 nm in the violet-blue region of the spectrum. In order to make the FMF fluorescent, we doped CDs with N heteroatoms, as previously detailed (Arcudi et al., 2016). We treated the material through hydrothermal synthesis in 10 mL of water, with natural SF playing dual roles as a carbon source and support material and urea acting as a nitrogen source. Nucleation resulted from the thermal carbonization of precursors in the solution, then the heteroatom is doped through a high temperature synthesis process, significantly enhancing the PL signal of CDs (Miao et al., 2020). Therefore, the nuclei expanded because of additional molecules diffusing to the CD surface.

3.3. Characterization of FMF-based hybrid ink for 3D printing

To make FMF suitable for practical printing, it was mixed with PVA or PEG – depending on the extrusion approach. PEG is a synthetic hydrogel that is commonly used in 3D printing due to its hydrophilic properties as well as its customizable chemical structure (Chiappone et al., 2016). In this work, PEG was used to prepare a FMF-PEG composite ink for aligned 3D printing. PVA is another highly hydrophilic, inexpensive polymer that has been approved by the United States Food and Drug Administration for medical use (Baker et al., 2012; DeMerlis and Schoneker, 2003), making it a suitable FMF composite component for syringe extrusion.

The selection of polyvinyl alcohol (PVA) and polyethylene glycol (PEG) as components in this application is related to their properties as

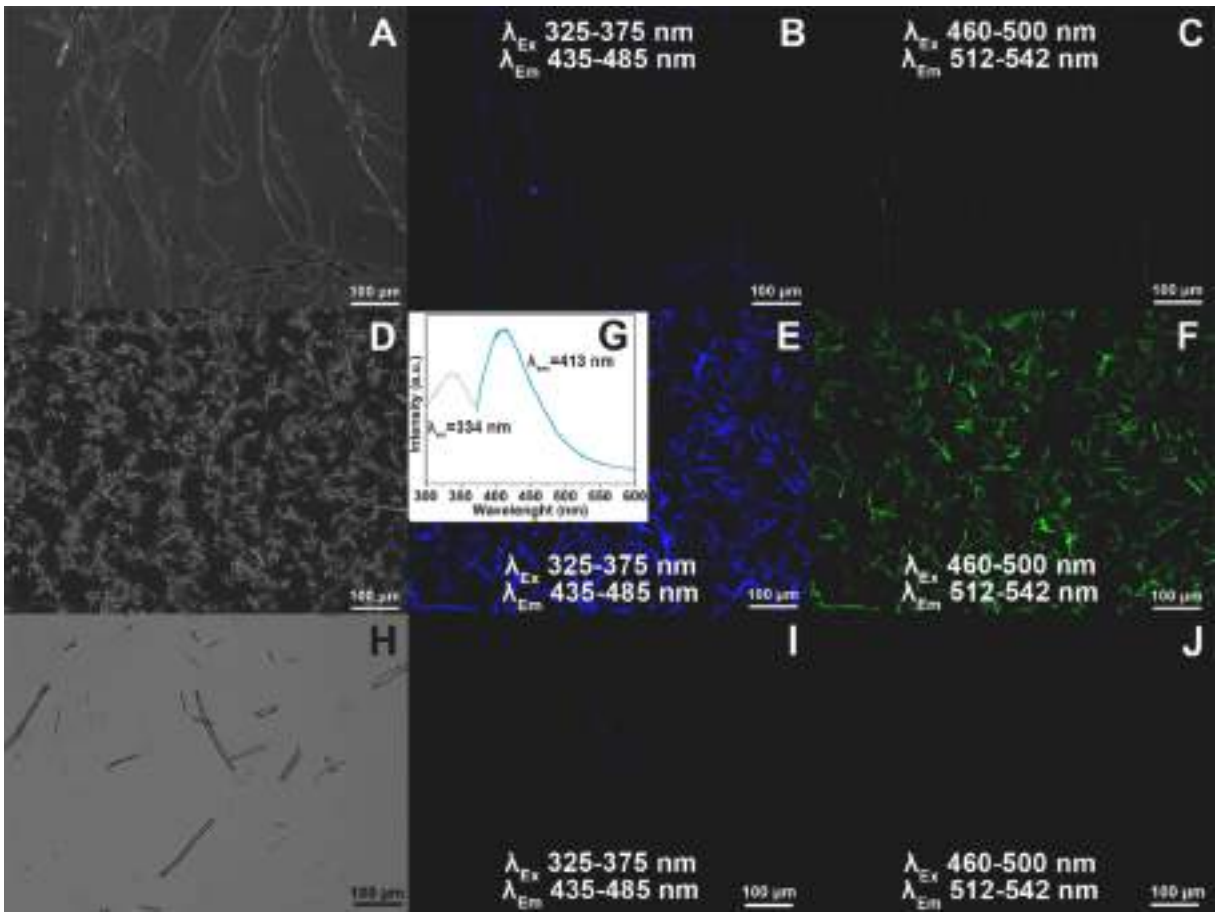

Fig. 3. Fluorescent microscopy images of (A-C) SF, (D-F) FMF and (H-J) FMF obtained by hydrothermal synthesis without urea. Images A, D – phase contrast; B, E, I – DAPI channel (DAPI); C, F, J – FITC channel (FITC), H - bright field. (G) PL spectrum under an excitation wavelength of 334 nm with emission at 413 nm for FMF.

biodegradable packaging materials. These polymers are widely considered viable alternatives to conventional plastics in packaging, which often lack the desired functional properties. The packaging industry increasingly prioritizes research in the field of biodegradable, optically active materials that possess superior mechanical characteristics and their further practical implementation (Yousefi et al., 2019).

PVA's ability to form thin films is a key factor in the creation of invisible tags (Oun et al., 2022). The sequential application of FMF-PVA and PVA layers enables the desired optical properties, resulting in tags that are invisible in daylight but easily detectable under UV light.

PEG, characterized by its low polydispersity index, ensures the preservation of the optically active properties within the final structure, independent of adverse effects caused by polydispersity (Hu and Liu, 2022). Additionally, PEG's ease of optimization as an ink component enhances the system's practical applicability.

Since composite ink properties depend on polymer base and microfiber filler material properties as well as interactions between both constituents and filler material arrangement in the matrix, nonlinear rotational experiments were conducted to generate flow curves for the FMF-PVA and FMF-PEG samples, as shown in (Fig. 4**A,B**). Comparing

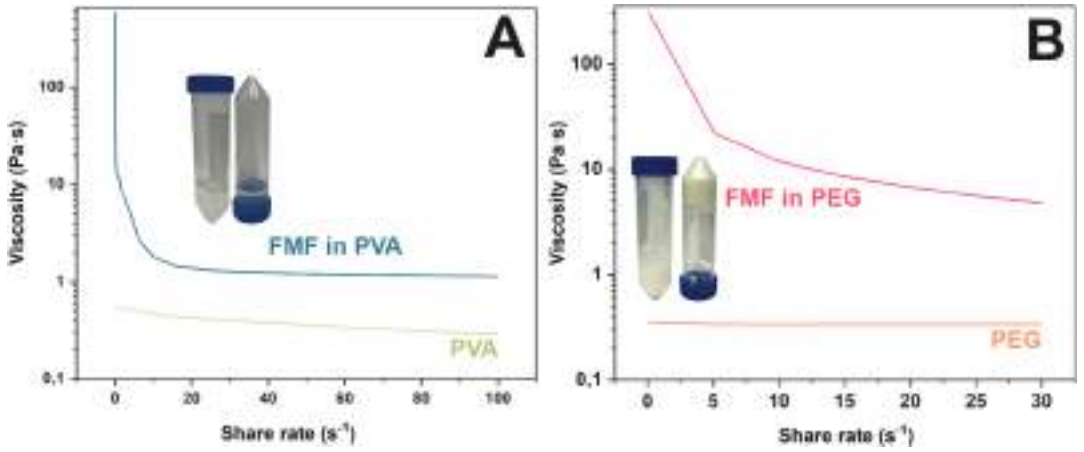

Fig. 4. (A) Variation in FMF-PVA ink viscosity plotted as a function of shear rate at 20 °C and (B) FMF-PEG ink viscosity plotted as a function of shear rate at 40 °C.

the inks based on FMF and unmodified polymers, no shear-thinning behavior was observed in the case of neat polymers, which confirms that the inks qualify as non-Newtonian and are suitable for 3D gel printing.

Both examined inks demonstrated inelastic behavior, as evidenced by G' being less than G″. The values reported as 1.53×10^{-7} and 6.02×10^{-5} for PEG. The G' and G″ values for the PVA-based ink were determined to be 1.81×10^{-6} and 3.58×10^{-5}, respectively. The Young's modulus of the inks was calculated to be 1.81×10^{-4} for FMF-PEG and 1.07×10^{-4} for FMF-PVA. These results further confirm the elastic behavior of the obtained inks, which is essential for their applicability in printing. Both inks displayed shear thinning properties, where viscosity decreased as shear rate increased, which is advantageous for 3D printing (Khuu et al., 2019; Morozova et al., 2021). Between them, the FMF-PVA ink had higher viscosity, as shown in Fig. 4**A**. The viscosity curve of the FMF-PVA ink dropped significantly as shear rate increased from 0.01 to 30 s^{-1}, reaching a viscosity value of approximately 5 Pa·s. An important peculiarity of the FMF-PVA ink is its non-stability, as the flip test in Fig. 4**A** shows. Inks containing PVA harden in air during extrusion from a syringe onto a substrate. The FMF-PEG ink had an apparent viscosity of almost 1 Pa·s and significant shear thinning behaviour across the shear rate range from 10 to 100 s^{-1} (Fig. 4**B**). Fig. 4**B** also shows the FMF-PEG hybrid ink flip test at room temperature (22 °C), which indicates its stability. All the produced inks are still functional, 1 year after synthesis. The PVA-based inks gel only after exposure to open air and can be recovered through reheating. PEG-based inks are solid at room temperature, and are supposed to be used after heating, so it does not gel under normal conditions.

The ability to control the arrangement of microfibers in FMF-PVA composite inks extruded using a syringe was also investigated. This approach could provide a unique advantage for tailoring the design of printed materials by creating unique labels without the need for special conditions or equipment. When tested, a considerable degree of fiber alignment in the direction of extrusion was visible in the produced samples, which indicates the anisotropy of the resulting material. However, because of the additional layer of PVA coating on top of the pattern, both the printed pattern and the oriented FMF are not visible in daylight, as shown in Fig. 5**A**. The printed pattern is clearly visible only in ultraviolet irradiation due to the PL of FMF (Fig. 5**B**). Thus, we offer an effective approach to the development of unique printed patterns with various emission colours, which are urgently demanded due to their promising prospects in the next-generation anti-counterfeiting materials. Fig. 5**C** shows highly aligned clusters of microfibers at the macroscale in daylight and **Figure S5** demonstrates their optical activity under UV light.

A Cellink BIO X 3D printer was used to explore the connection between microfiber orientation and the parameters of the manufacturing process, which is an essential aspect in the development of 3D-printed polymer-matrix composite materials with customized material characteristics. Extrusion of the FMF-PEG ink was realized through the nozzle of the Cellink Bio X. This gives rise to aligned fibroin structures in the direction of flow and allows anisotropy, which is especially noticeable under UV light (Fig. 5**D,E).** An important advantage of this approach is the possibility to select the nozzle width, print speed, and pressure, which allows the number of FMF distributed across the print width to be controlled (Fig. 5**D-F**). One year after printing, PL microscopy images were obtained for both FMF-PVA and FMF-PEG inks, indicating that the inks are highly stable and capable of retaining their optical properties. Fig. 5**J-L** demonstrates that there is no degradation of FMF optical properties after 12 months of storage.

4. Conclusion

In this work, we produced stimuli-responsive luminescent tags able to show encrypted messages under UV light that are easy to incorporate into packaging for potential anti-counterfeiting applications due to their difficult-to-replicate unique optical properties. FMF covered with violet/blue-emissive fluorescent CD (λ_{em} = 413 nm) were obtained by hydrothermal synthesis using SF, which acted as both a carbon source and a substrate, and the $-NH_2$ functional groups in urea as a nitrogen heteroatom source. Using a Cellink BIO X printer and a syringe, we demonstrated two working approaches of FMF-PVA and FMF-PEG extrusion, respectively. Both approaches demonstrated the uniform distribution and alignment of 100 μm FMF during the printing process, meeting the requirements of complex design, high-speed production, straightforward operation, and hidden images security features. Due to

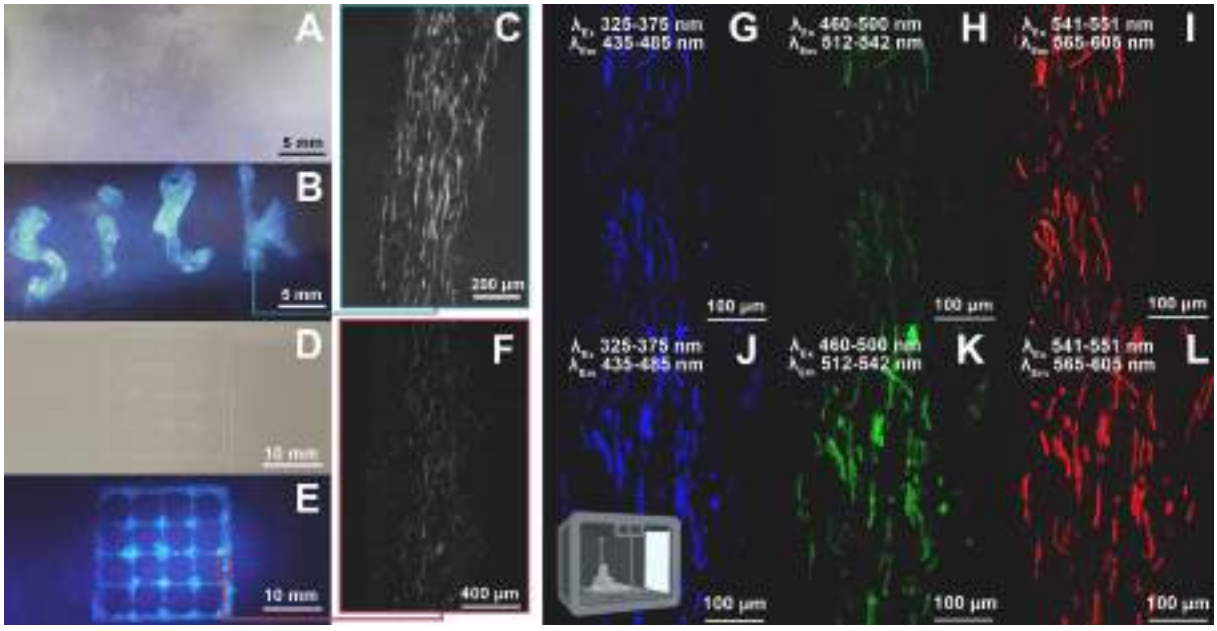

Fig. 5. Images of FMF-PVA sample extruded through a syringe under (A) natural light and (B) UV light. (C) Optical microscopy image of FMF-PVA sample. Images of 3D-printed FMF-PEG sample under (D) natural light and (E) UV light. (F) Optical microscopy image of FMF-PEG sample. Fluorescent microscopy images demonstrates that there is no degradation of FMF optical properties after 12 months of storage of FMF-PVA sample extruded through a syringe (G-I) and 3D-printed FMF-PEG sample (J-L). Images G, J – DAPI channel (DAPI), H, K – FITC channel (FITC), I, L – Cy5 channel (Cy5).

the alignment of FMF in the PVA or PEG polymer matrix upon extrusion, the final material has unique structural and functional characteristics that cannot be attained by each component individually. Merging luminescence and oriented 3D printing of FMF-based inks would greatly improve anti-counterfeiting security measures, enabling the creation of safe and unique labels for security printing. This approach can be applied in 3D printing and rapid prototyping to enhance the production of layered composite materials with embedded microfiber patterns.

Author contributions

The manuscript was written through contributions of all authors. All authors have given approval to the final version of the manuscript.

CRediT authorship contribution statement

Anastasia Kryuchkova: Writing – original draft, Visualization, Investigation. **Anna Ponomarets:** Writing – original draft, Methodology, Investigation. **Victoriia Suchilova:** Methodology, Investigation, Conceptualization. **Egor Ryabchenko:** Investigation, Methodology, Visualization, Writing – original draft. **Chantal Tracey:** Writing – review & editing, Supervision, Project administration. **Pavel Krivoshapkin:** Writing – review & editing, Supervision, Resources, Project administration, Funding acquisition, Conceptualization. **Elena Krivoshapkina:** Writing – review & editing, Supervision, Resources, Project administration, Funding acquisition, Conceptualization.

Declaration of competing interest

The authors declare that they have no known competing financial interests or personal relationships that could have appeared to influence the work reported in this paper.

Acknowledgment

This work was supported by the Russian Ministry of Science and Higher Education “Science and Universities” National Project state task N№ FSER-2022-0002. E.F.K. also acknowledges the Priority 2030 Federal Academic Leadership Program for infrastructural support.

Appendix A. Supplementary data

Supplementary data to this article can be found online at https://doi.org/10.1016/j.ces.2024.120868.

Data availability

Data will be made available on request.

References

Arcudi, F., Dordevic, L., Prato, M., 2016. Synthesis, separation, and characterization of small and highly fluorescent nitrogen-doped carbon nanodots. Angew. Chem. - Int. Ed. 55, 2107–2112. https://doi.org/10.1002/anie.201510158.

Baker, M.I., Walsh, S.P., Schwartz, Z., Boyan, B.D., 2012. A review of polyvinyl alcohol and its uses in cartilage and orthopedic applications. J. Biomed. Mater. Res. - Part B Appl. Biomater. 100 B, 1451–1457. https://doi.org/10.1002/jbm.b.32694.

Barth, A., 2000. The infrared absorption of amino acid side chains. Prog. Biophys. Mol. Biol. 74, 141–173. https://doi.org/10.1016/S0079-6107(00)00021-3.

Blanco, I., 2020. The use of composite materials in 3d printing. J. Compos. Sci. 4. https://doi.org/10.3390/jcs4020042.

Bucciarelli, A., Greco, G., Corridori, I., Pugno, N.M., Motta, A., 2021. A design of experiment rational optimization of the degumming process and its impact on the silk fibroin properties. ACS Biomater. Sci. Eng. 7, 1374–1393. https://doi.org/10.1021/acsbiomaterials.0c01657.

Chang, K., Liu, Z., Chen, H., Sheng, L., Zhang, S.X.A., Chiu, D.T., Yin, S., Wu, C., Qin, W., 2014. Conjugated polymer dots for ultra-stable full-color fluorescence patterning. Small 10, 4270–4275. https://doi.org/10.1002/smll.201401436.

Chekini, M., Prince, E., Zhao, L., Mundoor, H., Smalyukh, I.I., Kumacheva, E., 2020. Chiral carbon dots synthesized on cellulose nanocrystals. Adv. Opt. Mater. 8. https://doi.org/10.1002/adom.201901911.

Chen, F., Porter, D., Vollrath, F., 2012. Morphology and structure of silkworm cocoons. Mater. Sci. Eng. C 32, 772–778. https://doi.org/10.1016/j.msec.2012.01.023.

Chiappone, A., Fantino, E., Roppolo, I., Lorusso, M., Manfredi, D., Fino, P., Pirri, C.F., Calignano, F., 2016. 3D printed PEG-based hybrid nanocomposites obtained by sol-gel technique. ACS Appl. Mater. Interfaces 8, 5627–5633. https://doi.org/10.1021/acsami.5b12578.

DeMerlis, C.C., Schoneker, D.R., 2003. Review of the oral toxicity of polyvinyl alcohol (PVA). Food Chem. Toxicol. 41, 319–326. https://doi.org/10.1016/S0278-6915(02)00258-2.

Dong, A., Huang, P., Caughey, W.S., 1990. Protein secondary structures in water from second-derivative amide I infrared spectra. Biochemistry 29, 3303–3308. https://doi.org/10.1021/bi00465a022.

Dou, H., Zuo, B., 2015. Effect of sodium carbonate concentrations on the degumming and regeneration process of silk fibroin. J. Text. Inst. 106, 311–319. https://doi.org/10.1080/00405000.2014.919065.

Du, Y., Guo, S., 2016. Chemically doped fluorescent carbon and graphene quantum dots for bioimaging, sensor, catalytic and photoelectronic applications. Nanoscale 8, 2532–2543. https://doi.org/10.1039/c5nr07579c.

Fernando, K.A.S., Sahu, S., Liu, Y., Lewis, W.K., Guliants, E.A., Jafariyan, A., Wang, P., Bunker, C.E., Sun, Y.P., 2015. Carbon quantum dots and applications in photocatalytic energy conversion. ACS Appl. Mater. Interfaces 7, 8363–8376. https://doi.org/10.1021/acsami.5b00448.

Gamo, T., Inokuchi, T., Laufer, H., 1977. Polypeptides of fibroin and sericin secreted from the different sections of the silk gland in Bombyx mori. Insect Biochem. 7, 285–295. https://doi.org/10.1016/0020-1790(77)90026-9.

Gao, R., Fang, X., Yan, D., 2019. Recent developments in stimuli-responsive luminescent films. J. Mater. Chem. C 7, 3399–3412. https://doi.org/10.1039/c9tc00348g.

Geminiani, L., Campione, F.P., Canevali, C., Corti, C., Giussani, B., Gorla, G., Luraschi, M., Recchia, S., Rampazzi, L., 2023. Historical silk: a novel method to evaluate degumming with non-invasive infrared spectroscopy and spectral deconvolution. Materials (Basel) 16. https://doi.org/10.3390/ma16051819.

Guo, B., Ma, P.X., 2014. Synthetic biodegradable functional polymers for tissue engineering: a brief review. Sci. China Chem. 57, 490–500. https://doi.org/10.1007/s11426-014-5086-y.

Guo, C., Zhang, J., Jordan, J.S., Wang, X., Henning, R.W., Yarger, J.L., 2018. Structural comparison of various silkworm silks: an insight into the structure-property relationship. Biomacromolecules 19, 906–917. https://doi.org/10.1021/acs.biomac.7b01687.

Gupta, B.K., Haranath, D., Saini, S., Singh, V.N., Shanker, V., 2010. Synthesis and characterization of ultra-fine Y2O 3:Eu^{3+} nanophosphors for luminescent security ink applications. Nanotechnology 21. https://doi.org/10.1088/0957-4484/21/5/055607.

Haggag, K., El-Sayed, H., Allam, O.G., 2007. Degumming of silk using microwave-assisted treatments. J. Nat. Fibers 4, 1–22. https://doi.org/10.1300/J395v04n03_01.

Han, T., Yuan, Y., Liang, X., Zhang, Y., Xiong, C., Dong, L., 2017. Colloidal stable quantum dots modified by dual functional group polymers for inkjet printing. J. Mater. Chem. C 5, 4629–4635. https://doi.org/10.1039/c7tc00452d.

Hola, K., Zhang, Y., Wang, Y., Giannelis, E.P., Zboril, R., Rogach, A.L., 2014. Carbon dots - Emerging light emitters for bioimaging, cancer therapy and optoelectronics. Nano Today 9, 590–603. https://doi.org/10.1016/j.nantod.2014.09.004.

Horan, R.L., Antle, K., Collette, A.L., Wang, Y., Huang, J., Moreau, J.E., Volloch, V., Kaplan, D.L., Altman, G.H., 2005. In vitro degradation of silk fibroin. Biomaterials 26, 3385–3393. https://doi.org/10.1016/j.biomaterials.2004.09.020.

Hussin, H., Soin, N., Wan Muhamad Hatta, S.F., Md Rezali, F.A., Abdul Wahab, Y., 2021. Review—recent progress in the diversity of inkjet-printed flexible sensor structures in biomedical engineering applications. J. Electrochem. Soc. 168, 077508. https://doi.org/10.1149/1945-7111/ac0e4b.

Jackson, M., Mantsch, H.H., 1995. The use and misuse of FTIR spectroscopy in the determination of protein structure. Crit. Rev. Biochem. Mol. Biol. 30, 95–120. https://doi.org/10.3109/10409239509085140.

Jarošová, R., McClure, S.E., Gajda, M., Jović, M., Girault, H.H., Lesch, A., Maiden, M., Waters, C., Swain, G.M., 2019. Inkjet-printed carbon nanotube electrodes for measuring pyocyanin and uric acid in a wound fluid simulant and culture media. Anal. Chem. 91, 8835–8844. https://doi.org/10.1021/acs.analchem.8b05591.

Jia, Z., Gong, J., Zeng, Y., Ran, J., Liu, J., Wang, K., Xie, C., Lu, X., Wang, J., 2021. Bioinspired conductive silk microfiber integrated bioelectronic for diagnosis and wound healing in diabetes. Adv. Funct. Mater. 31. https://doi.org/10.1002/adfm.202010461.

Jiang, K., Sun, S., Zhang, L., Lu, Y., Wu, A., Cai, C., Lin, H., 2015. Red, green, and blue luminescence by carbon dots: full-color emission tuning and multicolor cellular imaging. Angew. Chem. 127, 5450–5453. https://doi.org/10.1002/ange.201501193.

Jiang, K., Zhang, L., Lu, J., Xu, C., Cai, C., Lin, H., 2016. Triple-mode emission of carbon dots: applications for advanced anti-counterfeiting. Angew. Chem. - Int. Ed. 55, 7231–7235. https://doi.org/10.1002/anie.201602445.

Jiang, K., Wang, Y., Cai, C., Lin, H., 2017. Activating room temperature long afterglow of carbon dots via covalent fixation. Chem. Mater. 29, 4866–4873. https://doi.org/10.1021/acs.chemmater.7b00831.

Johansson, S.G.O., Wüthrich, B., Zortea-Caflisch, C., 1985. Nightly asthma caused by allergens in silkfilled bed quilts: clinical and immunologic studies. J. Allergy Clin. Immunol. 75, 452–459. https://doi.org/10.1016/S0091-6749(85)80017-8.

Jung, C., 2000. Insight into protein structure and protein-ligand recognition by Fourier transform infrared spectroscopy. J. Mol. Recognit. 13, 325–351. https://doi.org/10.1002/1099-1352(200011/12)13:6<325::AID-JMR507>3.0.CO;2-C.
Kaczmarek, A.M., Liu, Y.Y., Wang, C., Laforce, B., Vincze, L., Van Der Voort, P., Van Hecke, K., Van Deun, R., 2017. Lanthanide "chameleon" multistage anti-counterfeit materials. Adv. Funct. Mater. 27. https://doi.org/10.1002/adfm.201700258.
Kalytchuk, S., Wang, Y., Poláková, K., Zbořil, R., 2018. Carbon dot fluorescence-lifetime-encoded anti-counterfeiting. ACS Appl. Mater. Interfaces 10, 29902–29908. https://doi.org/10.1021/acsami.8b11663.
Kasoju, N., Bora, U., 2012. Silk fibroin in tissue engineering. Adv. Healthc. Mater. 1, 393–412. https://doi.org/10.1002/adhm.201200097.
Khuu, N., Alizadehgiashi, M., Gevorkian, A., Galati, E., Yan, N., Kumacheva, E., 2019. Temperature-mediated microfluidic extrusion of structurally anisotropic hydrogels. Adv. Mater. Technol. 4. https://doi.org/10.1002/admt.201800627.
Kim, U.J., Park, J., Joo Kim, H., Wada, M., Kaplan, D.L., 2005. Three-dimensional aqueous-derived biomaterial scaffolds from silk fibroin. Biomaterials 26, 2775–2785. https://doi.org/10.1016/j.biomaterials.2004.07.044.
Kiseleva, A., Nestor, G., Östman, J.R., Kriuchkova, A., Savin, A., Krivoshapkin, P., Krivoshapkina, E., Seisenbaeva, G.A., Kessler, V.G., 2021. Modulating surface properties of the Linothele fallax spider web by solvent treatment. Biomacromolecules 22, 4945–4955. https://doi.org/10.1021/acs.biomac.1c00787.
Koh, L.D., Cheng, Y., Teng, C.P., Khin, Y.W., Loh, X.J., Tee, S.Y., Low, M., Ye, E., Yu, H. D., Zhang, Y.W., Han, M.Y., 2015. Structures, mechanical properties and applications of silk fibroin materials. Prog. Polym. Sci. 46, 86–110. https://doi.org/10.1016/j.progpolymsci.2015.02.001.
Koperska, M.A., Pawcenis, D., Bagniuk, J., Zaitz, M.M., Missori, M., Łojewski, T., Łojewska, J., 2014. Degradation markers of fibroin in silk through infrared spectroscopy. Polym. Degrad. Stab. 105, 185–196. https://doi.org/10.1016/j.polymdegradstab.2014.04.008.
Krykpayev, B., Farooqui, M.F., Bilal, R.M., Vaseem, M., Shamim, A., 2017. A wearable tracking device inkjet-printed on textile. Microelectronics J. 65, 40–48. https://doi.org/10.1016/j.mejo.2017.05.010.
Kryuchkova, A., Savin, A., Kiseleva, A., Dukhinova, M., Krivoshapkina, E., Krivoshapkin, P., 2023. Magnetothermal spider silk-based scaffolds for cartilage regeneration. Int. J. Biol. Macromol. 253. https://doi.org/10.1016/j.ijbiomac.2023.127246.
Kumar, S.V., Kumar, S.P., Rupesh, D., Nitin, K., 2011. Comparative conformational, structural and vibrational study on the molecular structure of tyrosine and L-DOPA using density functional theory. J. Chem. Pharm. Res. 3, 675–684.
Laity, P.R., Gilks, S.E., Holland, C., 2015. Rheological behaviour of native silk feedstocks. Polymer (Guildf) 67, 28–39. https://doi.org/10.1016/j.polymer.2015.04.049.
Li, M., Ogiso, M., Minoura, N., 2003. Enzymatic degradation behavior of porous silk fibroin sheets. Biomaterials 24, 357–365. https://doi.org/10.1016/S0142-9612(02)00326-5.
Li, Q., Ohulchanskyy, T.Y., Liu, R., Koynov, K., Wu, D., Best, A., Kumar, R., Bonoiu, A., Prasad, P.N., 2010. Photoluminescent carbon dots as biocompatible nanoprobes for targeting cancer cells in vitro. J. Phys. Chem. C 114, 12062–12068. https://doi.org/10.1021/jp911539r.
Li, J., Rossignol, F., Macdonald, J., 2015. Inkjet printing for biosensor fabrication: combining chemistry and technology for advanced manufacturing. Lab Chip 15, 2538–2558. https://doi.org/10.1039/c5lc00235d.
Li, W., Zhang, Z., Kong, B., Feng, S., Wang, J., Wang, L., Yang, J., Zhang, F., Wu, P., Zhao, D., 2013. Simple and green synthesis of nitrogen-doped photoluminescent carbonaceous nanospheres for bioimaging. Angew. Chem. - Int. Ed. 52, 8151–8155. https://doi.org/10.1002/anie.201303927.
Lin, Y., Chen, J., Tavakoli, M.M., Gao, Y., Zhu, Y., Zhang, D., Kam, M., He, Z., Fan, Z., 2019. Printable fabrication of a fully integrated and self-powered sensor system on plastic substrates. Adv. Mater. 31. https://doi.org/10.1002/adma.201804285.
Lucas, F., Shaw, J.T.B., Smith, S.G., 1958. The silk fibroins. Adv. Protein Chem. 13, 107–242. https://doi.org/10.1016/S0065-3233(08)60599-9.
Lucas, F., Shaw, J.T.B., Smith, S.G., 1960. Comparative studies of fibroins: I. The amino acid composition of various fibroins and its significance in relation to their crystal structure and taxonomy. J. Mol. Biol. 2, 339–349. https://doi.org/10.1016/S0022-2836(60)80045-9.
Luo, P.G., Sahu, S., Yang, S.T., Sonkar, S.K., Wang, J., Wang, H., Lecroy, G.E., Cao, L., Sun, Y.P., 2013. Carbon "quantum" dots for optical bioimaging. J. Mater. Chem. B 1, 2116–2127. https://doi.org/10.1039/c3tb00018d.
Ma, H., Li, J., Zhou, J., Luo, Q., Wu, W., Mao, Z., Ma, W., 2022. Screen-printed carbon black/recycled sericin@fabrics for wearable sensors to monitor sweat loss. ACS Appl. Mater. Interfaces 14, 11813–11819. https://doi.org/10.1021/acsami.1c23341.
Ma, Y., She, P., Zhang, K.Y., Yang, H., Qin, Y., Xu, Z., Liu, S., Zhao, Q., Huang, W., 2018. Dynamic metal-ligand coordination for multicolour and water-jet rewritable paper. Nat. Commun. 9. https://doi.org/10.1038/s41467-017-02452-w.
Madurga, R., Gañán-Calvo, A.M., Plaza, G.R., Guinea, G.V., Elices, M., Pérez-Rigueiro, J., 2017. Straining flow spinning: production of regenerated silk fibers under a wide range of mild coagulating chemistries. Green Chem. 19, 3380–3389. https://doi.org/10.1039/c7gc01254c.
Maltseva, E.S., Nikolaeva, V.O., Savin, A.M., Dobryakov, M.Y., Koshel, E.I., Krivoshapkin, P.V., Krivoshapkina, E.F., 2022. Fluorescent hybrid material based on natural spider silk and carbon dots for bioapplication. ACS Biomater. Sci. Eng. 8, 3310–3319. https://doi.org/10.1021/acsbiomaterials.2c00322.
Mandal, B.B., Grinberg, A., Gil, E.S., Panilaitis, B., Kaplan, D.L., 2012. High-strength silk protein scaffolds for bone repair. Proc. Natl. Acad. Sci. USA 109, 7699–7704. https://doi.org/10.1073/pnas.1119474109.
Miao, S., Liang, K., Zhu, J., Yang, B., Zhao, D., Kong, B., 2020. Hetero-atom-doped carbon dots: doping strategies, properties and applications. Nano Today 33. https://doi.org/10.1016/j.nantod.2020.100879.
Molinnus, D., Drinic, A., Iken, H., Kröger, N., Zinser, M., Smeets, R., Köpf, M., Kopp, A., Schöning, M.J., 2021. Towards a flexible electrochemical biosensor fabricated from biocompatible Bombyx mori silk. Biosens. Bioelectron. 183. https://doi.org/10.1016/j.bios.2021.113204.
Morozova, S.M., Statsenko, T.G., Ryabchenko, E.O., Gevorkian, A., Adibnia, V., Lozhkin, M.S., Kireynov, A.V., Kumacheva, E., 2021. Multicolored nanocolloidal hydrogel inks. Adv. Funct. Mater. 31. https://doi.org/10.1002/adfm.202105470.
Mouro, C., Jung, C., Bondon, A., Simonneaux, G., 1997. Comparative Fourier transform infrared studies of the secondary structure and the CO heme ligand environment in cytochrome P-450cam and cytochrome P-420cam. Biochemistry 36, 8125–8134. https://doi.org/10.1021/bi9700173.
Muthamma, K., Sunil, D., Shetty, P., 2021. Carbon dots as emerging luminophores in security inks for anti-counterfeit applications - An up-to-date review. Appl. Mater. Today 23. https://doi.org/10.1016/j.apmt.2021.101050.
Oun, A.A., Shin, G.H., Rhim, J.W., Kim, J.T., 2022. Recent advances in polyvinyl alcohol-based composite films and their applications in food packaging. Food Packag. Shelf Life 34. https://doi.org/10.1016/j.fpsl.2022.100991.
Peng, Z., Han, X., Li, S., Al-Youbi, A.O., Bashammakh, A.S., El-Shahawi, M.S., Leblanc, R. M., 2017. Carbon dots: biomacromolecule interaction, bioimaging and nanomedicine. Coord. Chem. Rev. 343, 256–277. https://doi.org/10.1016/j.ccr.2017.06.001.
Peng, H.Q., Sun, C.L., Niu, L.Y., Chen, Y.Z., Wu, L.Z., Tung, C.H., Yang, Q.Z., 2016. Supramolecular polymeric fluorescent nanoparticles based on quadruple hydrogen bonds. Adv. Funct. Mater. 26, 5483–5489. https://doi.org/10.1002/adfm.201600593.
Pérez-Rigueiro, J., Elices, M., Llorca, J., Viney, C., 2002. Effect of degumming on the tensile properties of silkworm (Bombyx mori) silk fiber. J. Appl. Polym. Sci. 84, 1431–1437. https://doi.org/10.1002/app.10366.
Qi, Y., Wang, H., Wei, K., Yang, Y., Zheng, R.Y., Kim, I.S., Zhang, K.Q., 2017. A review of structure construction of silk fibroin biomaterials from single structures to multi-level structures. Int. J. Mol. Sci. 18. https://doi.org/10.3390/ijms18030237.
Qiu, R., Wang, K., Tian, H., Liu, X., Liu, G., Hu, Z., Zhao, L., 2022. Analysis on the printability and rheological characteristics of bigel inks: potential in 3D food printing. Food Hydrocoll. 129. https://doi.org/10.1016/j.foodhyd.2022.107675.
Qu, S., Wang, X., Lu, Q., Liu, X., Wang, L., 2012. A biocompatible fluorescent ink based on water-soluble luminescent carbon nanodots. Angew. Chem. - Int. Ed. 51, 12215–12218. https://doi.org/10.1002/anie.201206791.
Quitain, A.T., Daimon, H., Fujie, K., Katoh, S., Moriyoshi, T., 2006. Microwave-assisted hydrothermal degradation of silk protein to amino acids. Ind. Eng. Chem. Res. 45, 4471–4474. https://doi.org/10.1021/ie0580699.
Roblin, N.V., DeBari, M.K., Shefter, S.L., Iizuka, E., Abbott, R.D., 2023. Development of a more environmentally friendly silk fibroin scaffold for soft tissue applications. J. Funct. Biomater. 14. https://doi.org/10.3390/jfb14040230.
Rosati, G., Urban, M., Zhao, L., Yang, Q., de Carvalho Castro e Silva, C., Bonaldo, S., Parolo, C., Nguyen, E.P., Ortega, G., Fornasiero, P., Paccagnella, A., Merkoçi, A., 2022. A plug, print & play inkjet printing and impedance-based biosensing technology operating through a smartphone for clinical diagnostics. Biosens. Bioelectron. 196. https://doi.org/10.1016/j.bios.2021.113737.
Sahoo, S., Lok Toh, S., Hong Goh, J.C., 2010. PLGA nanofiber-coated silk microfibrous scaffold for connective tissue engineering. J. Biomed. Mater. Res. - Part B Appl. Biomater. 95, 19–28. https://doi.org/10.1002/jbm.b.31678.
Sai Saran, O., Prudhvidhar Reddy, A., Chaturya, L., Pavan Kumar, M., 2022. 3D printing of composite materials: a short review. Mater. Today Proc. 64, 615–619. https://doi.org/10.1016/j.matpr.2022.05.144.
Seal, B.L., Otero, T.C., Panitch, A., 2001. Polymeric biomaterials for tissue and organ regeneration. Mater. Sci. Eng. R Rep. 34, 147–230. https://doi.org/10.1016/S0927-796X(01)00035-3.
Seo, S.J., Das, G., Shin, H.S., Patra, J.K., 2023. Silk sericin protein materials: characteristics and applications in food-sector industries. Int. J. Mol. Sci. 24. https://doi.org/10.3390/ijms24054951.
Singh, K.P., Jayasomu, R.S., 2002. Bombyx mori - A review of its potential as a medicinal insect. Pharm. Biol. 40, 28–32. https://doi.org/10.1076/phbi.40.1.28.5857.
Song, Z., Lin, T., Lin, L., Lin, S., Fu, F., Wang, X., Guo, L., 2016. Invisible security ink based on water-soluble graphitic carbon nitride quantum dots. Angew. Chem. - Int. Ed. 55, 2773–2777. https://doi.org/10.1002/anie.201510945.
Sun, L.W., Shi, H.Q., Li, W.N., Xiao, H.M., Fu, S.Y., Cao, X.Z., Li, Z.X., 2012. Lanthanum-doped ZnO quantum dots with greatly enhanced fluorescent quantum yield. J. Mater. Chem. 22, 8221–8227. https://doi.org/10.1039/c2jm00040g.
Taddei, P., Monti, P., 2005. Vibrational infrared conformational studies of model peptides representing the semicrystalline domains of Bombyx mori silk fibroin. Biopolymers 78, 249–258. https://doi.org/10.1002/bip.20275.
Taddei, P., Pavoni, E., Tsukada, M., 2016. Stability toward alkaline hydrolysis of B. mori silk fibroin grafted with methacrylamide. J. Raman Spectrosc. 47, 731–739. https://doi.org/10.1002/jrs.4892.
Tao, H., Kaplan, D.L., Omenetto, F.G., 2012. Silk materials - A road to sustainable high technology. Adv. Mater. 24, 2824–2837. https://doi.org/10.1002/adma.201104477.
Teramoto, H., Miyazawa, M., 2005. Molecular orientation behavior of silk sericin film as revealed by ATR infrared spectroscopy. Biomacromolecules 6, 2049–2057. https://doi.org/10.1021/bm0500547.
Tian, Z., Zhang, X., Li, D., Zhou, D., Jing, P., Shen, D., Qu, S., Zboril, R., Rogach, A.L., 2017. Full-color inorganic carbon dot phosphors for white-light-emitting diodes. Adv. Opt. Mater. 5. https://doi.org/10.1002/adom.201700416.

Titirici, M.M., Antonietti, M., 2010. Chemistry and materials options of sustainable carbon materials made by hydrothermal carbonization. Chem. Soc. Rev. 39, 103–116. https://doi.org/10.1039/b819318p.

Tofail, S.A.M., Koumoulos, E.P., Bandyopadhyay, A., Bose, S., O'Donoghue, L., Charitidis, C., 2018. Additive manufacturing: scientific and technological challenges, market uptake and opportunities. Mater. Today 21, 22–37. https://doi.org/10.1016/j.mattod.2017.07.001.

Tomal, W., Świergosz, T., Pilch, M., Kasprzyk, W., Ortyl, J., 2021. New horizons for carbon dots: quantum nano-photoinitiating catalysts for cationic photopolymerization and three-dimensional (3D) printing under visible light. Polym. Chem. 12, 3661–3676. https://doi.org/10.1039/d1py00228g.

Tracey, C.T., Kryuchkova, A.V., Bhatt, T.K., Krivoshapkin, P.V., Krivoshapkina, E.F., 2023. Silk for post-harvest horticultural produce safety and quality control. J. Food Eng. 337. https://doi.org/10.1016/j.jfoodeng.2022.111231.

Tretinnikov, O.N., Tamada, Y., 2001. Influence of casting temperature on the near-surface structure and wettability of cast silk fibroin films. Langmuir 17, 7406–7413. https://doi.org/10.1021/la010791y.

Van De Weert, M., Haris, P.I., Hennink, W.E., Crommelin, D.J.A., 2001. Fourier transform infrared spectrometric analysis of protein conformation: effect of sampling method and stress factors. Anal. Biochem. 297, 160–169. https://doi.org/10.1006/abio.2001.5337.

Vepari, C., Kaplan, D.L., 2007. Silk as a biomaterial. Prog. Polym. Sci. 32, 991–1007. https://doi.org/10.1016/j.progpolymsci.2007.05.013.

Wang, H.Y., Chen, Y.Y., Zhang, Y.Q., 2015. Processing and characterization of powdered silk micro- and nanofibers by ultrasonication. Mater. Sci. Eng. C 48, 444–452. https://doi.org/10.1016/j.msec.2014.12.028.

Wang, L., Li, B., Xu, F., Li, Y., Xu, Z., Wei, D., Feng, Y., Wang, Y., Jia, D., Zhou, Y., 2017. Visual in vivo degradation of injectable hydrogel by real-time and non-invasive tracking using carbon nanodots as fluorescent indicator. Biomaterials 145, 192–206. https://doi.org/10.1016/j.biomaterials.2017.08.039.

Wang, K., Ma, Q., Zhou, H.T., Zhao, J.M., Cao, M., Wang, S.D., 2023. Review on fabrication and application of regenerated Bombyx mori silk fibroin materials. Autex Res. J. 23, 164–183. https://doi.org/10.2478/aut-2021-0059.

Wang, H.Y., Zhang, Y.Q., Wei, Z.G., 2021. Dissolution and processing of silk fibroin for materials science. Crit. Rev. Biotechnol. 41, 406–424. https://doi.org/10.1080/07388551.2020.1853030.

West, J.L., Hubbell, J.A., 1999. Polymeric biomaterials with degradation sites for proteases involved in cell migration. Macromolecules 32, 241–244. https://doi.org/10.1021/ma981296k.

Wilson, D., Valluzzi, R., Kaplan, D., 2000. Conformational transitions model silk peptides. Biophys. J. 78, 2690–2701. https://doi.org/10.1016/S0006-3495(00)76813-5.

Yan, F., Jiang, Y., Sun, X., Wei, J., Chen, L., Zhang, Y., 2020. Multicolor carbon dots with concentration-tunable fluorescence and solvent-affected aggregation states for white light-emitting diodes. Nano Res. 13, 52–60. https://doi.org/10.1007/s12274-019-2569-3.

Yao, Y., Guan, D., Zhang, C., Liu, J., Zhu, X., Huang, T., Liu, J., Cui, H., Tang, K.L., Lin, J., Li, F., 2022. Silkworm spinning inspired 3D printing toward a high strength scaffold for bone regeneration. J. Mater. Chem. B 10, 6946–6957. https://doi.org/10.1039/d2tb01161a.

Yin, Y., Zeng, Y., Chen, X., Fan, Y., 2016. The internet of things in healthcare: an overview. J. Ind. Inf. Integr. 1, 3–13. https://doi.org/10.1016/j.jii.2016.03.004.

Yoon, B., Lee, J., Park, I.S., Jeon, S., Lee, J., Kim, J.M., 2013. Recent functional material based approaches to prevent and detect counterfeiting. J. Mater. Chem. C 1, 2388–2403. https://doi.org/10.1039/c3tc00818e.

Zhang, P., Lan, J., Wang, Y., Xiong, Z.H., Huang, C.Z., 2015. Luminescent golden silk and fabric through in situ chemically coating pristine-silk with gold nanoclusters. Biomaterials 36, 26–32. https://doi.org/10.1016/j.biomaterials.2014.08.026.

Zhang, F., Lu, Q., Ming, J., Dou, H., Liu, Z., Zuo, B., Qin, M., Li, F., Kaplan, D.L., Zhang, X., 2014. Silk dissolution and regeneration at the nanofibril scale. J. Mater. Chem. B 2, 3879–3885. https://doi.org/10.1039/c3tb21582b.

Zhang, J., Yu, S.H., 2016. Carbon dots: large-scale synthesis, sensing and bioimaging. Mater. Today 19, 382–393. https://doi.org/10.1016/j.mattod.2015.11.008.

Zhang, X., Zhang, Y., Wang, Yu., Kalytchuk, S., Kershaw, S.V., Wang, Y., Wang, P., Zhang, T., Zhao, Y., Zhang, H., Cui, T., Wang, Y., Zhao, J., Yu, W.W., Rogach, A.L., 2013. Color-switchable electroluminescence of carbon dot light-emitting diodes. ACS Nano 7, 11234–11241. https://doi.org/10.1021/nn405017q.

Zhou, C., Shi, Y., Sun, C., Yu, S., Liu, M., Gao, C., 2014. Thin-film composite membranes formed by interfacial polymerization with natural material sericin and trimesoyl chloride for nanofiltration. J. Memb. Sci. 471, 381–391. https://doi.org/10.1016/j.memsci.2014.08.033.

Zhu, L., Lin, J., Pei, L., Luo, Y., Li, D., Huang, Z., 2022. Recent advances in environmentally friendly and green degumming processes of silk for textile and non-textile applications. Polymers (Basel) 14. https://doi.org/10.3390/polym14040659.